21 April 1994

PHYSICS LETTERS B

ELSEVIER

Physics Letters B 325 (1994) 521–525

Single top production at LEP 200

K. Hagiwara, M. Tanaka

Theory Group, KEK, Tsukuba, Ibaraki 305, Japan

T. Stelzer

Department of Physics, Durham University, DH1 3LE, Durham, UK

Received 20 January 1994
Editor: P.V. Landshoff

Abstract

We present exact tree level cross sections for the single top production process $e^-e^+ \to e^-\bar{\nu}_e t\bar{b}$ at LEP 200. The results reproduce roughly those obtained earlier by using the equivalent real photon approximation and we confirm the observation that detecting a top heavier than half the c.m. energy is not feasible at LEP 200. The calculation has been performed by a new automatic Feynman amplitude generator MadGraph which produces HELAS code for the helicity amplitudes.

The search for the top quark is a primary target of present and future collider experiments. For a top quark lighter than half the center of mass (c.m.) energy $\sqrt{s}$, top production at e^+e^- colliders will be dominated by the pair production process $e^+e^- \to t\bar{t}$. This is, however, unlikely to be the case at LEP 200 if the CDF bound [1] on the top mass of $m_t \gtrsim 120$ GeV is valid. We can expect copious production of $t\bar{t}$ pairs at LEP 200 only if the top decays mainly into exotic modes which would invalidate the above bounds from hadron collider experiments.

The standard top quark can still be produced singly at LEP 200 via the higher order processes

$$e^-e^+ \to W^-t\bar{b}, \tag{1}$$

if $m_t < \sqrt{s} - m_W - m_b$, and

$$e^-e^+ \to e^-\bar{\nu}_e t\bar{b}, \tag{2}$$

if $m_t < \sqrt{s} - m_b$. Recently it has been claimed that single top quark production can be discovered at LEP 200 up to $m_t \sim 165$ GeV [2]. Another work states that the cross section is much too small for LEP 200 to produce top quarks singly with its design luminosity [3]. The former calculation introduces an artificial cutoff to the single top quark production cross section which is singular in the massless electron limit. The latter calculation makes use of the equivalent real photon approximation (EPA) to estimate the cross section from that of the subprocess

$$\gamma e^+ \to \bar{\nu}_e t\bar{b}. \tag{3}$$

In order to resolve this conflict, we present in this report the exact tree level cross section for the single top quark production processes (1) and (2), and compare the latter cross section with that obtained by using the EPA. We find that the naive EPA as employed in Ref. [3] overestimates the cross section by about 30% and that one should expect even smaller cross sections than those estimated there. Therefore, we essentially confirm the observation of Panella et al. [3]

Elsevier Science B.V.
SSDI 0370-2693(94)00253-4

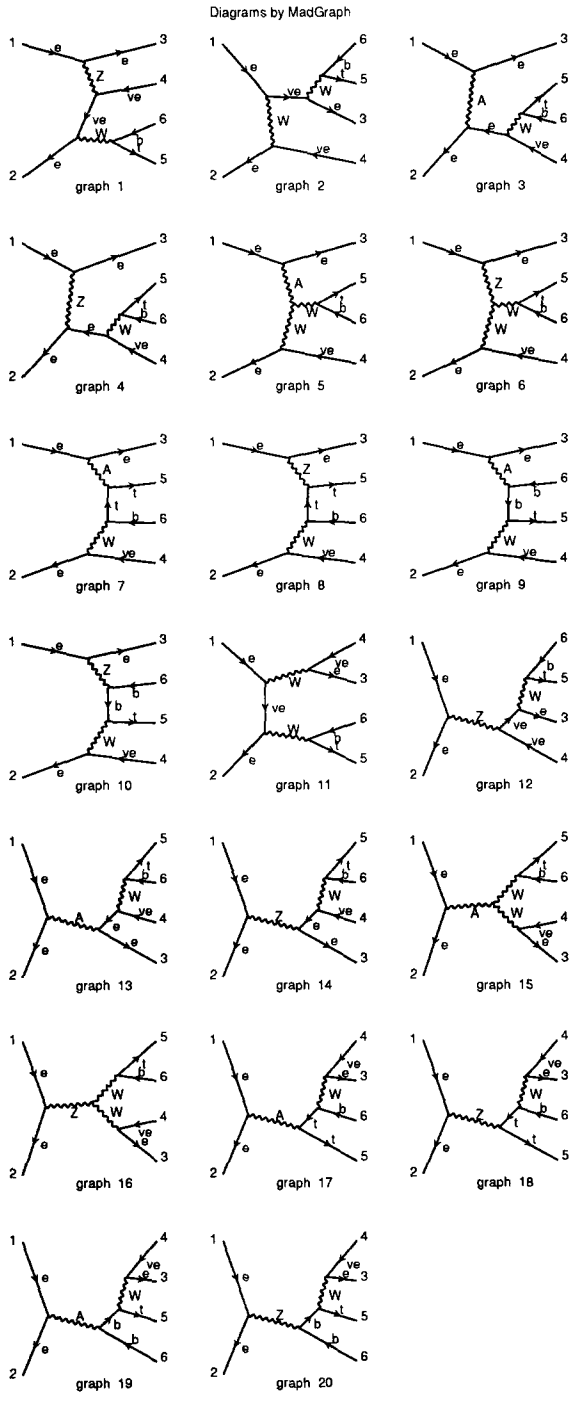

Fig. 1. Feynman diagrams for the process $e^-e^+ \to e^-\bar{\nu}_e t\bar{b}$ as generated by the automatic Feynman amplitude generator MadGraph [4].

that the single top production rate is too small to be interesting at LEP 200 with its planned luminosity of 0.5 fb^{-1}/year.

Our calculation has been performed by a recently completed automatic Feynman amplitude generator MadGraph [4]. Given the initial and final state particles for a Standard Model process, MadGraph automatically generates a postscript file of the Feynman graphs and a FORTRAN program of the helicity amplitudes that makes use of the HELAS subroutines [5]. We show in Fig. 1 the Feynman graphs of process (2) as generated by MadGraph. Differential cross sections can be easily obtained by integrating the squared matrix elements over the relevant phase space range.

It is not so trivial to obtain the total cross section of the process, because the matrix element becomes singular at high energies when the exchanged virtual photon in graphs 3, 5, 7 and 9 of Fig. 1 becomes nearly on-shell. The HELAS subroutines [5] numerically calculate the helicity amplitudes accurately in the singular region by modifying the $ee\gamma$ currents in the relevant diagrams and by choosing an appropriate parametrization of the phase space volume [6] such that no subtle cancellation occurs in the numerical program.

The results are shown in Fig. 2. Solid lines show the total cross sections for process (2) and dashed lines show those for process (1). In this calculation, we neglect the width of the top quark, and hence the cross sections are given only down to $m_t = \frac{1}{2}\sqrt{s} + 2$ GeV. Near the $t\bar{t}$ pair production threshold, one should examine the $e^+e^- \to b\bar{b}W^+W^-$ amplitudes carefully in the presence of the large non-perturbative QCD corrections [7]. In the helicity amplitudes for the process $e^-e^+ \to e^-\bar{\nu}_e t\bar{b}$, the so-called *annihilation* graphs 11–20 of Fig. 1 are a gauge invariant set. They contribute negligibly to the total cross section below the $e^-e^+ \to W^-t\bar{b}$ threshold, while they give just a fraction of the $e^-e^+ \to W^-t\bar{b}$ cross section above the threshold. The solid lines of Fig. 2 are obtained by consistently neglecting the contributions from the annihilation diagrams.

It is clear from Fig. 2 that the single top quark production cross section below the $e^-e^+ \to W^-t\bar{b}$ threshold is never greater than the 0.1 fb level at any conceivable LEP 200 energy, and that it remains

Table 1
Exact tree level cross sections for the process $e^-e^+ \to W^-t\bar{b}$ and the process $e^-e^+ \to e^-\bar{\nu}_e t\bar{b}$ at $\sqrt{s} = 190$ GeV for several top masses

m_t (Gev)	$\sigma(e^-e^+ \to W^-t\bar{b})$ (fb)	$\sigma(e^-e^+ \to e^-\bar{\nu}_e t\bar{b})$ (fb)
100	0.0050	0.046
110	–	0.027
120	–	0.016
130	–	0.0091
140	–	0.0044
150	–	0.0018
160	–	0.00048
170	–	0.000061

The $e^-e^+ \to e^-\bar{\nu}_e t\bar{b}$ cross sections are obtained by neglecting contributions from the *annihilation* diagrams 11–20 of Fig. 1. The SM parameters are chosen as follows: $m_b = 5$ GeV, $m_W = 80$ GeV, $m_Z = 91$ GeV, $e^2/4\pi = \sin^2\theta_W g^2/4\pi = 1/128$, and $\sin^2\theta_W = 0.23$. All the widths have been set to zero. The latter cross sections are obtained by multiplying the total cross sections by an overall factor 128/137 [6].

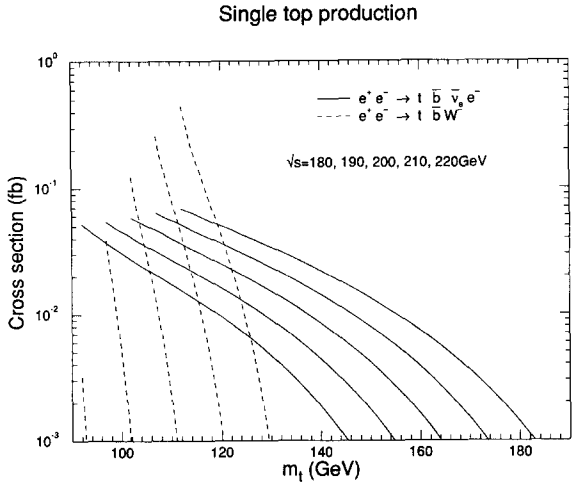

Fig. 2. Exact tree level cross sections for the process $e^-e^+ \to e^-\bar{\nu}_e t\bar{b}$ (solid lines) and the process $e^-e^+ \to W^-t\bar{b}$ (dashed lines) plotted against the top mass m_t at five c.m. energies $\sqrt{s}$ =180, 190, 200, 210, and 220 GeV. The solid lines are obtained by neglecting contributions from the *annihilation* diagrams 11–20 of Fig. 1. The SM parameters are chosen as follows: $m_b = 5$ GeV, $m_W = 80$ GeV, $m_Z = 91$ GeV, $e^2/4\pi = \sin^2\theta_W g^2/4\pi = 1/128$, and $\sin^2\theta_W = 0.23$. All the widths have been set to zero. The solid lines are obtained by multiplying the total cross sections by an overall factor 128/137 [6].

Table 2
Same as Table 1 but for the e^+e^- c.m. energy $\sqrt{s} = 200$ GeV

m_t (Gev)	$\sigma(e^-e^+ \to W^-t\bar{b})$ (fb)	$\sigma(e^-e^+ \to e^-\bar{\nu}_e t\bar{b})$ (fb)
110	0.0022	0.040
120	–	0.025
130	–	0.015
140	–	0.0085
150	–	0.0041
160	–	0.0016
170	–	0.00044
180	–	0.000056

below the level of a few times 0.1 fb even above the $e^-e^+ \to W^-t\bar{b}$ threshold. These observations confirm those of Ref. [3] qualitatively, and disagree with Ref. [2]. For the convenience of future comparison, we give some representative values of the total cross sections in Table 1 ($\sqrt{s} = 190$ GeV) and in Table 2 ($\sqrt{s} = 200$ GeV). The SM parameters are chosen as $m_b = 5$ GeV, $m_W = 80$ GeV, $m_Z = 91$ GeV, $e^2/4\pi = \sin^2\theta_W g^2/4\pi = 1/128$, $\sin^2\theta_W = 0.23$, and all the widths have been set to zero. The total cross section for the process $e^-e^+ \to e^-\bar{\nu}_e t\bar{b}$ is then multiplied by an overall factor of 128/137, since the cross section is dominated by the region of the phase space where the invariant mass of the virtual photon that couples to the external electron current is much smaller than one GeV [6]. Numerical errors associated with the Monte Carlo integration over the phase space volume are estimated to be less than 1% [8].

A closer comparison of our exact tree level results with the results using the equivalent real photon approximation (EPA) in Ref. [3], reveals that our exact cross section is consistently smaller than theirs by about 30%. To ensure that this is due to the approximation and not an error, we also calculate the cross section using the EPA.

Shown in Fig. 3 is the total cross section for the process $\gamma e^+ \to \bar{\nu}_e t\bar{b}$ as a function of the γe c.m. energy $\sqrt{s_{\gamma e}}$. The curves are calculated by using the MadGraph/HELAS system with the same SM parameters. The subprocess cross sections agree rather well with those reported in Ref. [3]. The validity of our calculation is further verified by comparing our result for a light top $m_t < m_W$, with the earlier result of Ref. [9].

Finally, in Fig. 4 we compare three estimates of the

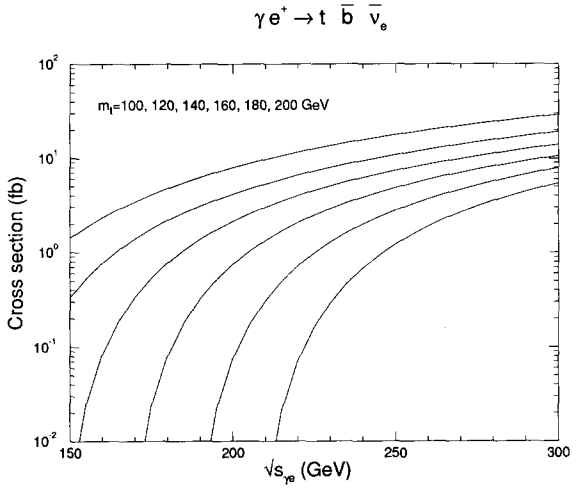

Fig. 3. Exact tree level cross sections for the process $\gamma e^+ \to \bar{\nu}_e t\bar{b}$ plotted against the γe c.m. energy $\sqrt{s_{\gamma e}}$ for six typical top mass m_t =100, 120, 140, 160, 180, and 200 GeV. The parameters are the same as those used in Fig. 2.

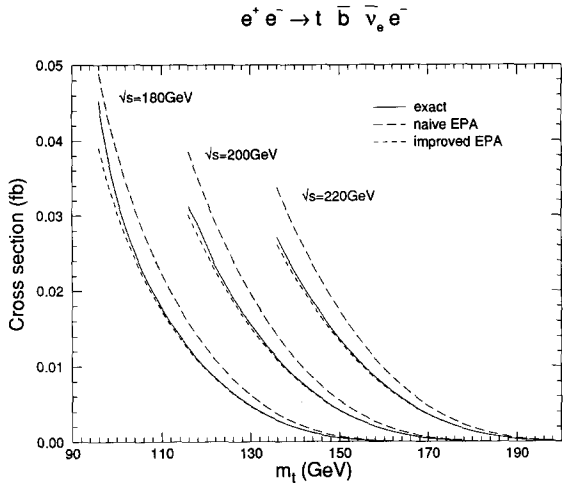

Fig. 4. Exact tree level cross sections for the process $e^-e^+ \to e^-\bar{\nu}_e t\bar{b}$ (solid lines) as compared with the cross sections obtained by the naive EPA (equivalent real photon approximation) of Ref. [3] (long dashed lines) and those by the improved EPA of Ref. [6] (short dashed lines). Here all the diagrams of Fig. 1 have been included in the exact cross sections. The parameters are the same as those used in Fig. 2.

total cross section for the process $e^-e^+ \to e^-\bar{\nu}_e t\bar{b}$. The solid lines are obtained by our exact tree level calculation. The long dashed lines are obtained by using the naive equivalent real photon distribution

$$D_{\gamma/e}(z,s)_{\text{naive EPA}} = \frac{\alpha}{2\pi}\frac{1+(1-z)^2}{z}\log\frac{s}{4m_e^2} \quad (4)$$

as adopted by Panella et al. [3]. And the short dashed lines are obtained by using the improved equivalent real photon ($\overline{\text{EPA}}$) distribution

$$D_{\gamma/e}(z,Q^2)_{\overline{\text{EPA}}} = \frac{\alpha}{2\pi}\left\{\frac{1+(1-z)^2}{z} \times \left[\log\frac{Q^2(1-z)}{m_e^2 z^2} - 1\right] + \frac{z}{2}\right\} \quad (5)$$

as proposed in Ref. [6]. Here the $\overline{\text{EPA}}$ flux of the photon is determined by respecting the exact lower kinematical limit of the virtual photon mass squared $t_{\min} = m_e^2 z^2/(1-z)^2$, whereas for the maximal virtuality Q^2 consistent with the real photon approximation, we take the typical virtuality scale of the subprocess $\gamma e^+ \to \bar{\nu}_e t\bar{b}$,

$$Q^2 = m_b^2 - (p_\gamma - p_b)^2. \quad (6)$$

The last term in the $\overline{\text{EPA}}$ distribution (5) without the logarithmic enhancement gives a small, but universal, contribution from the electron helicity flip amplitudes. Fig. 4 clearly shows that the naive EPA overestimates the cross section mainly because it fails to take account of the relatively small effective scale of the subprocess Q^2 (6). The improved EPA underestimates the cross section slightly because the exact cross section does not disappear when the virtual mass of the external electron current exceeds the scale (6). This is consistent with the $\overline{\text{EPA}}$ result as reported in Ref. [6] for the process $e^+e^- \to e^+e^-Z$.

The exact tree level cross sections of Fig. 4 (solid lines) are obtained by using all the diagrams of Fig. 1. One can observe the effects of the annihilation diagrams as small enhancements of the cross section near the $e^-e^+ \to W^-t\bar{b}$ threshold over the $\overline{\text{EPA}}$ estimates.

We conclude that our exact calculation of the single top production cross section is valid and that detecting a top heavier than half the c.m. energy is not feasible at LEP 200.

We wish to thank M. Sasaki for calling our attention to the discrepancy between Refs. [2] and [3]. We would also like to thank J. Kanzaki and I. Watanabe for helpful comments.

References

[1] CDF Collaboration, F. Abe et al.. , Phys. Rev. Lett. 68 (1992) 447; Phys. Rev. D 45 (1992) 3921; and talks presented at The 9th Topical Workshop on Proton Antiproton Collider Physics, Tsukuba (October 1993).
[2] M. Raidal and R. Vuopionperä, Phys. Lett. B 318 (1993) 237.
[3] O. Panella, G. Pancheri and Y.N. Srivastava, Phys. Lett. B 318 (1993) 241.
[4] T. Stelzer and W.F. Long, University of Wisconsin-Madison preprint MAD/PH/813 (January, 1994).
[5] H. Murayama, I. Watanabe and K. Hagiwara, HELAS: HELicity Amplitude Subroutines for Feynman Diagram Evaluations, KEK Report 91-11 (January, 1992).
[6] K. Hagiwara, H. Iwasaki, A. Miyamoto, H. Murayama and D. Zeppenfeld, Nucl. Phys. B 365 (1991) 544.
[7] V.S. Fadin and V.A. Khoze, JETP Lett. 46 (1987) 417; M. Strassler and M. Peskin, Phys. Rev. D 43 (1991) 1500; Y. Sumino, K. Fujii, K. Hagiwara, H. Murayama and C.K. Ng, Phys. Rev. D 47 (1993) 56.
[8] S. Kawabata, Comput. Phys. Commun. 41 (1986) 127.
[9] M. Katuya, J. Morishita, T. Munehisa and Y. Shimizu, Prog. Theor. Phys. 75 (1986) 92.